

## Supporting Information

### **Ru–Support Interface Tailoring for Enhanced Aerobic Oxidation of 1,4-Butanediol**

Shufang Zhang\*, Peipei Lang, Xue Bai, Wenjin Zhen, Lili Zhao, Yongxiang Zhao  
Engineering Research Center of Ministry of Education for Fine Chemicals Shanxi  
University Taiyuan, 030006, China;

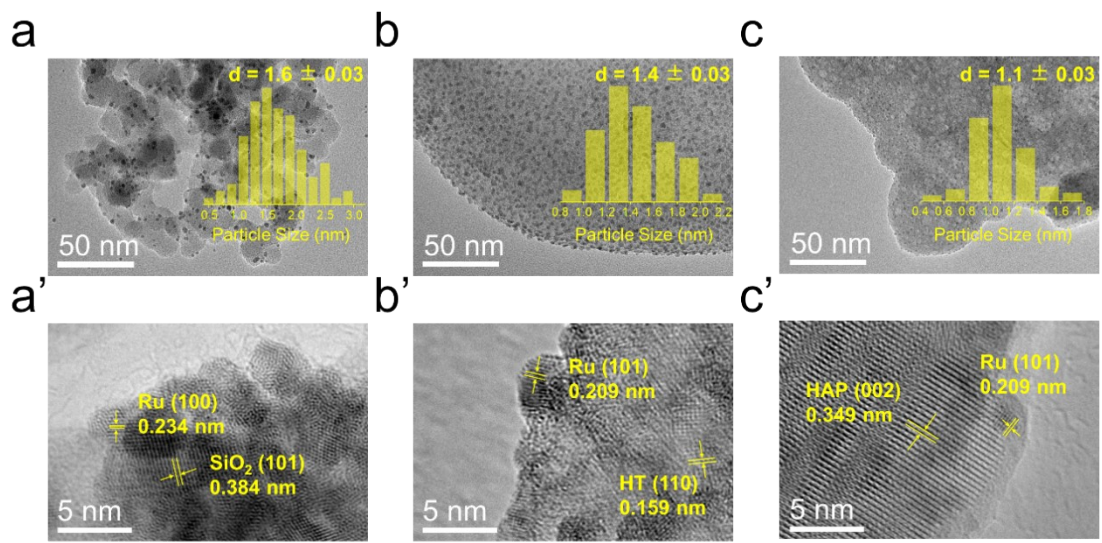


Figure S1. TEM and HRTEM images of Ru/SiO<sub>2</sub> (a-a'), Ru/HT (b-b'), Ru/HAP (c-c').

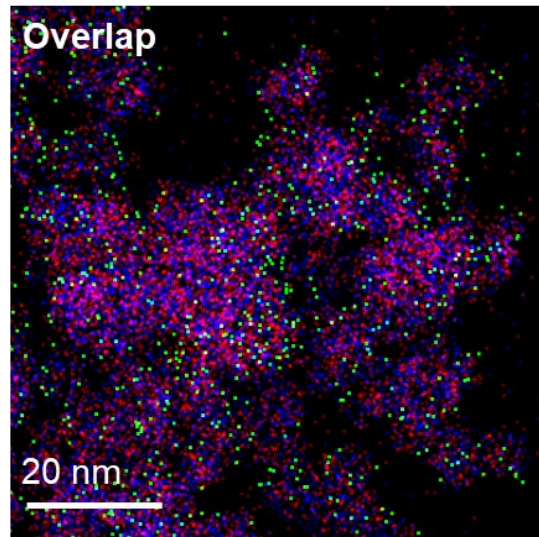


Figure S2. Overlay of Ru, Ti, and O elemental maps obtained by STEM-EDX analysis.

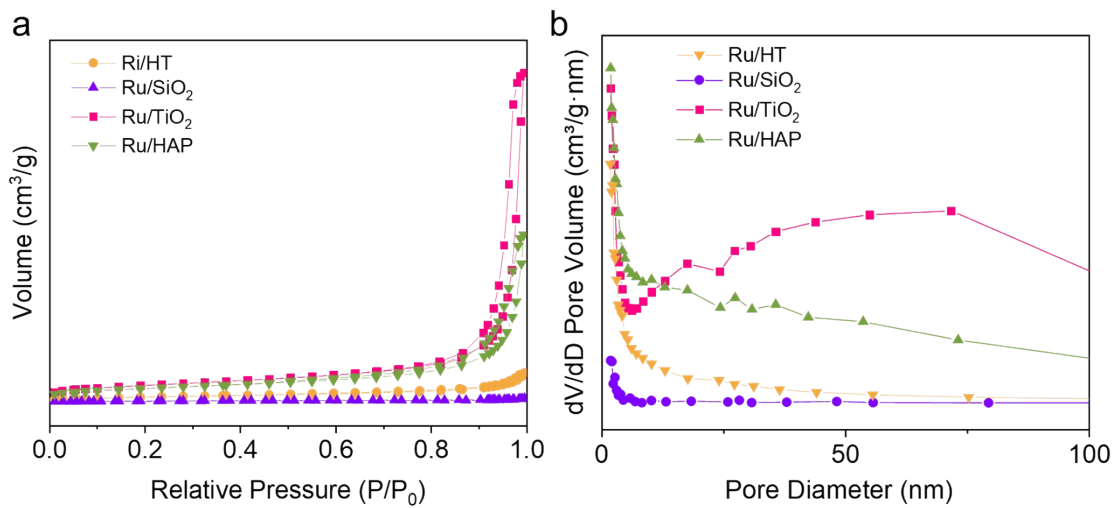


Figure S3. (a)  $N_2$  adsorption-desorption isotherms of the Ru-Support Interface catalyst. (b) Pore size distribution plot.

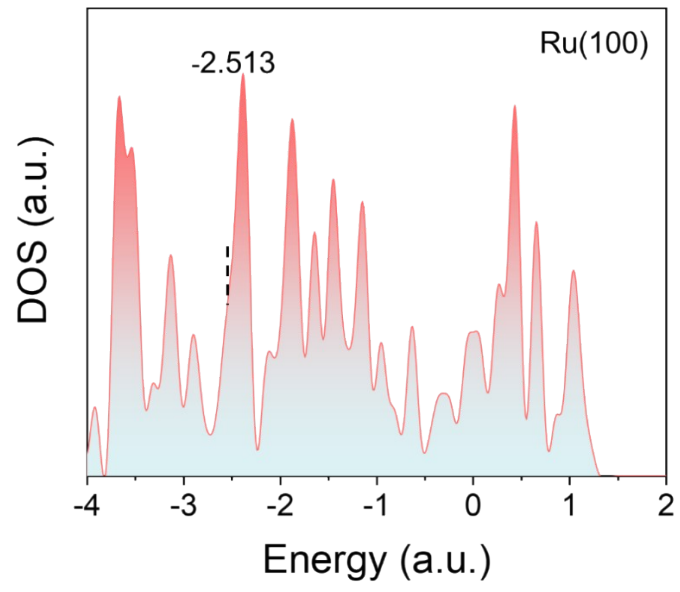


Figure S4. Analysis of DOS of Ru(100) model surface.

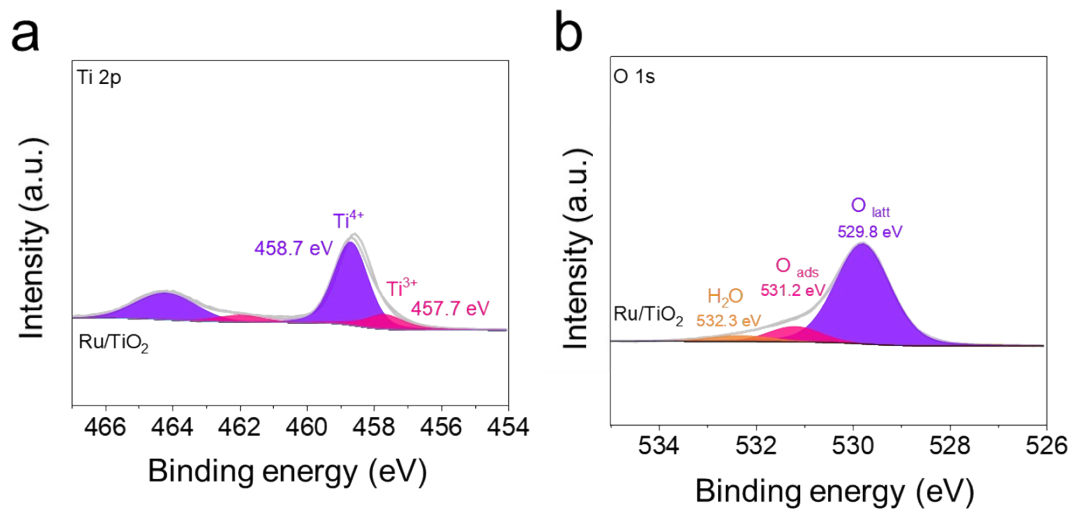


Figure S5. (a) Ti 2p and (b) O 1s XPS spectra of the Ru/TiO<sub>2</sub> catalyst.

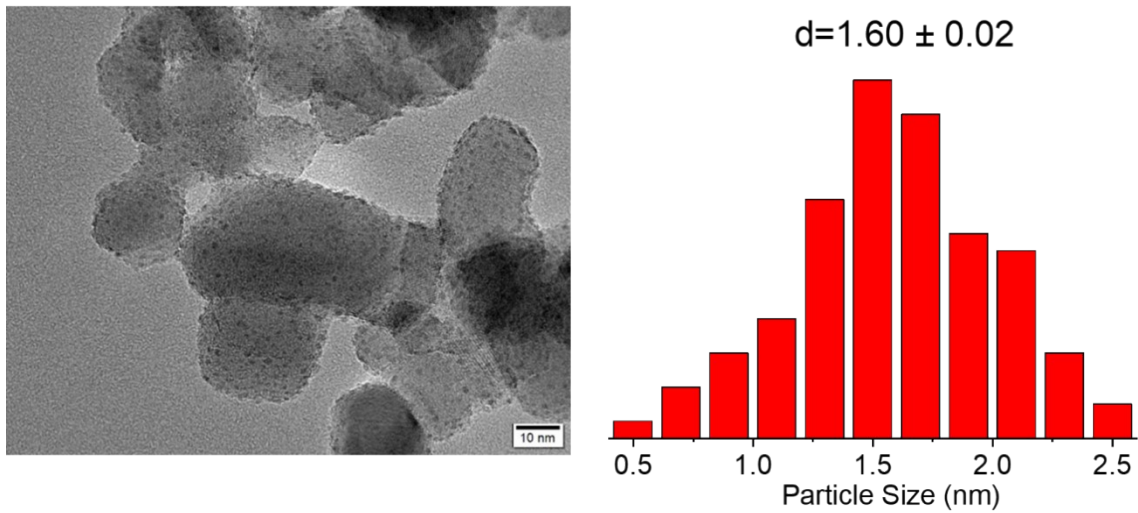


Figure S6. TEM image of Ru/TiO<sub>2</sub> after reaction and the corresponding particle size.

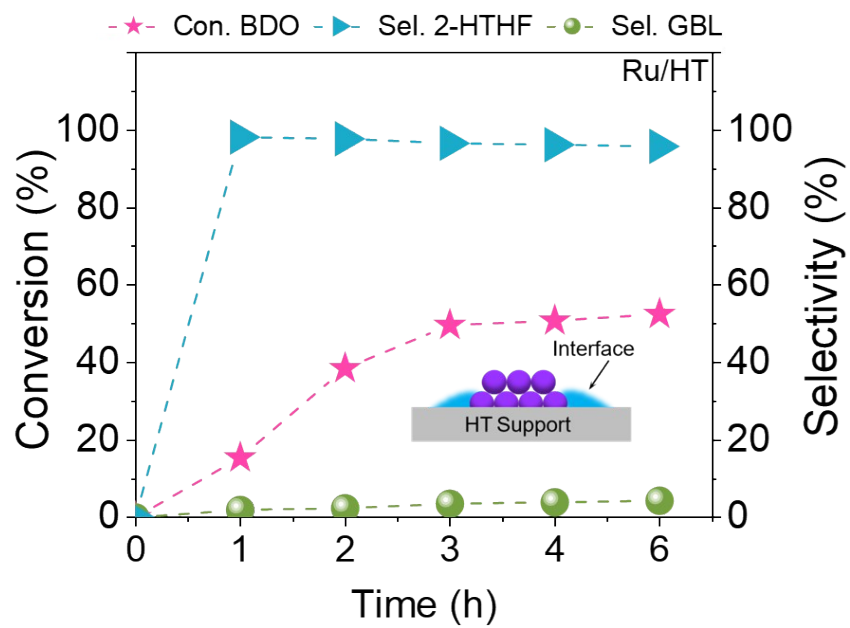


Figure S7. Kinetic Study of the Ru/HT catalyst.

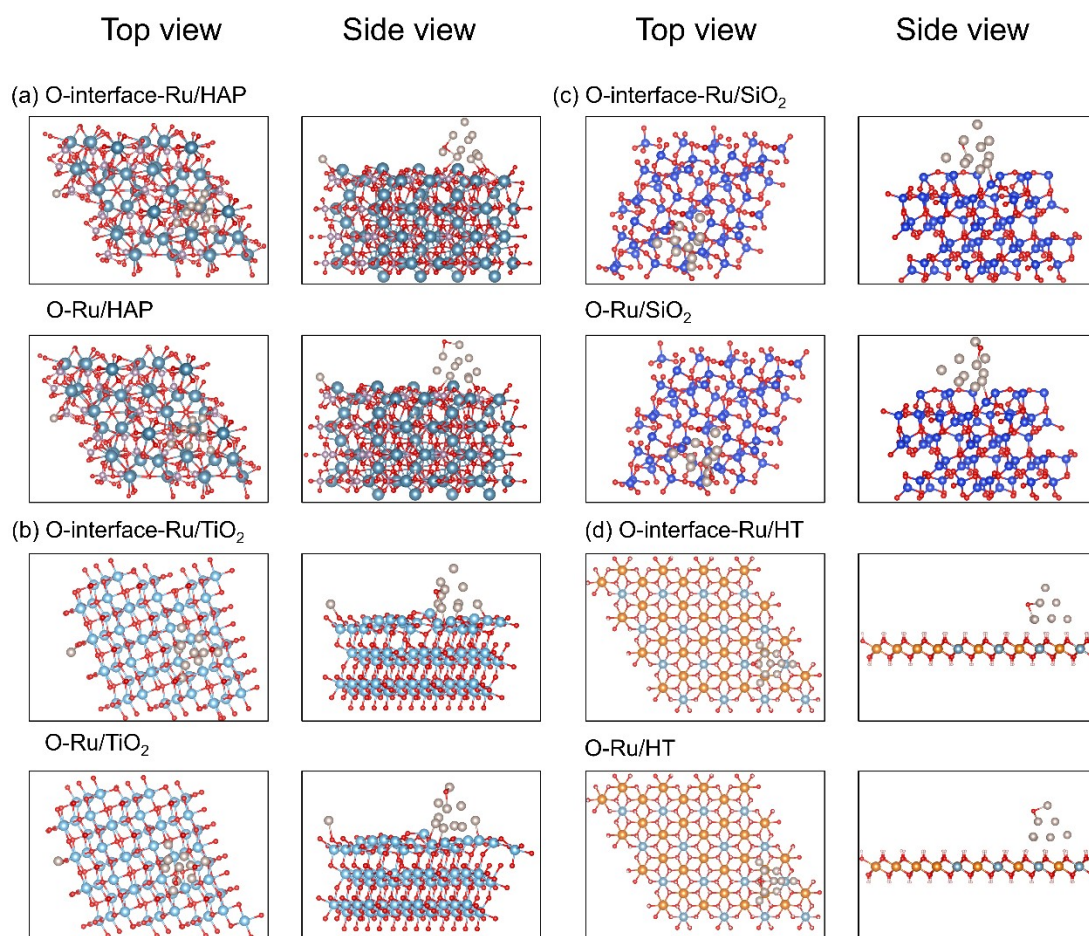


Figure S8. Top and side views of adsorption geometries of O atom on (a) Ru/HAP, (b) Ru/TiO<sub>2</sub>, (c) Ru/SiO<sub>2</sub>, (d) Ru/HT model surface, respectively.

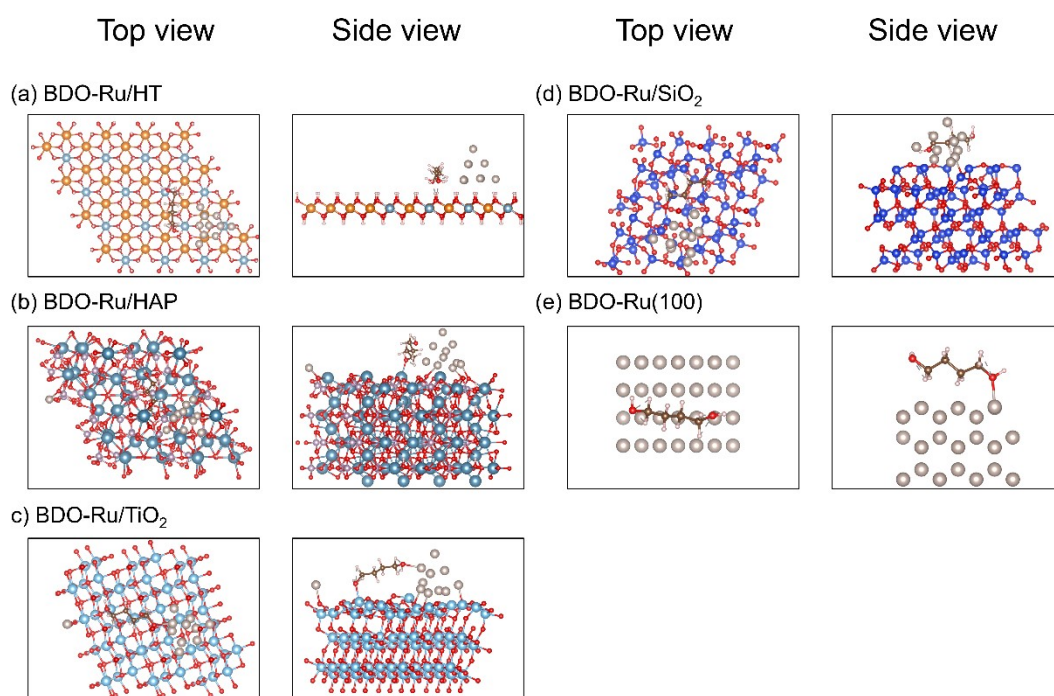


Figure S9. Top and side views of adsorption geometries of BDO on (a) Ru/HAP, (b) Ru/TiO<sub>2</sub>, (c) Ru/SiO<sub>2</sub>, (d) Ru/HT, (e) Ru(100) model surface, respectively.

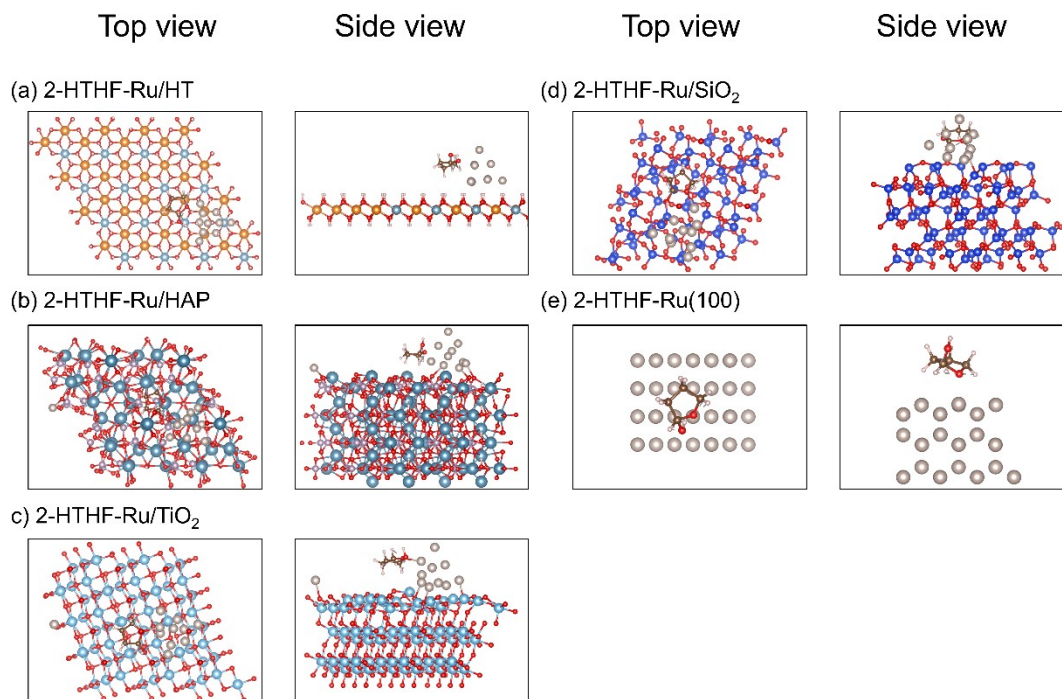


Figure S10. Top and side views of adsorption geometries of 2-HTHF on (a) Ru/HT, (b) Ru/HAP, (c) Ru/TiO<sub>2</sub>, (d) Ru/SiO<sub>2</sub>, (e) Ru(100) model surface, respectively.

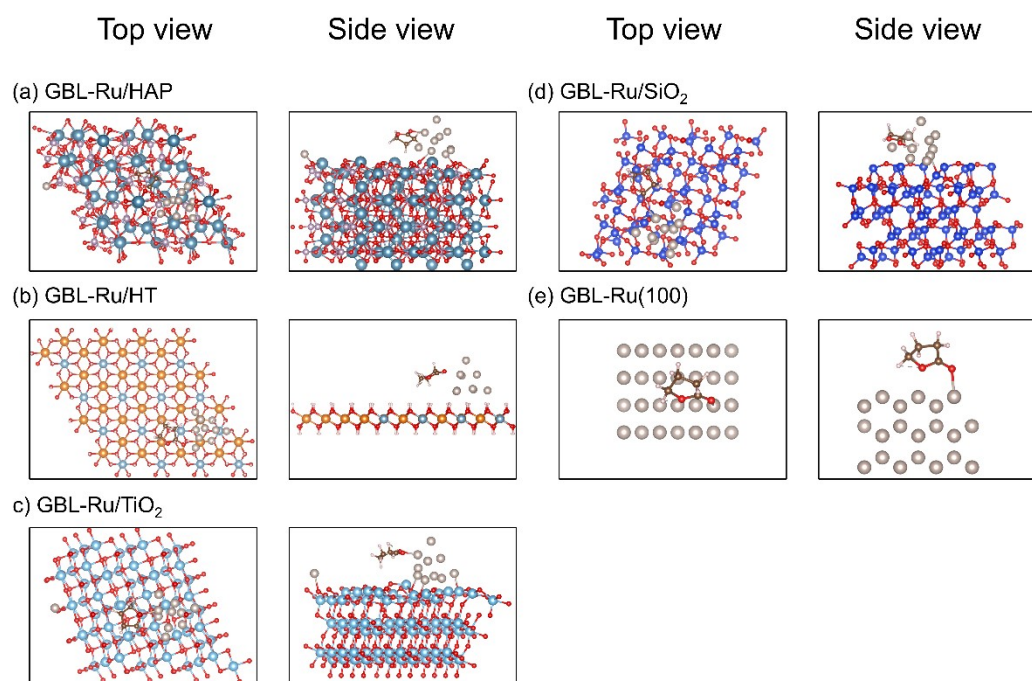


Figure S11. Top and side views of adsorption geometries of 2-HTHF on (a) Ru/HAP, (b) Ru/HT, (c) Ru/TiO<sub>2</sub>, (d) Ru/SiO<sub>2</sub>, (e) Ru(100) model surface, respectively.

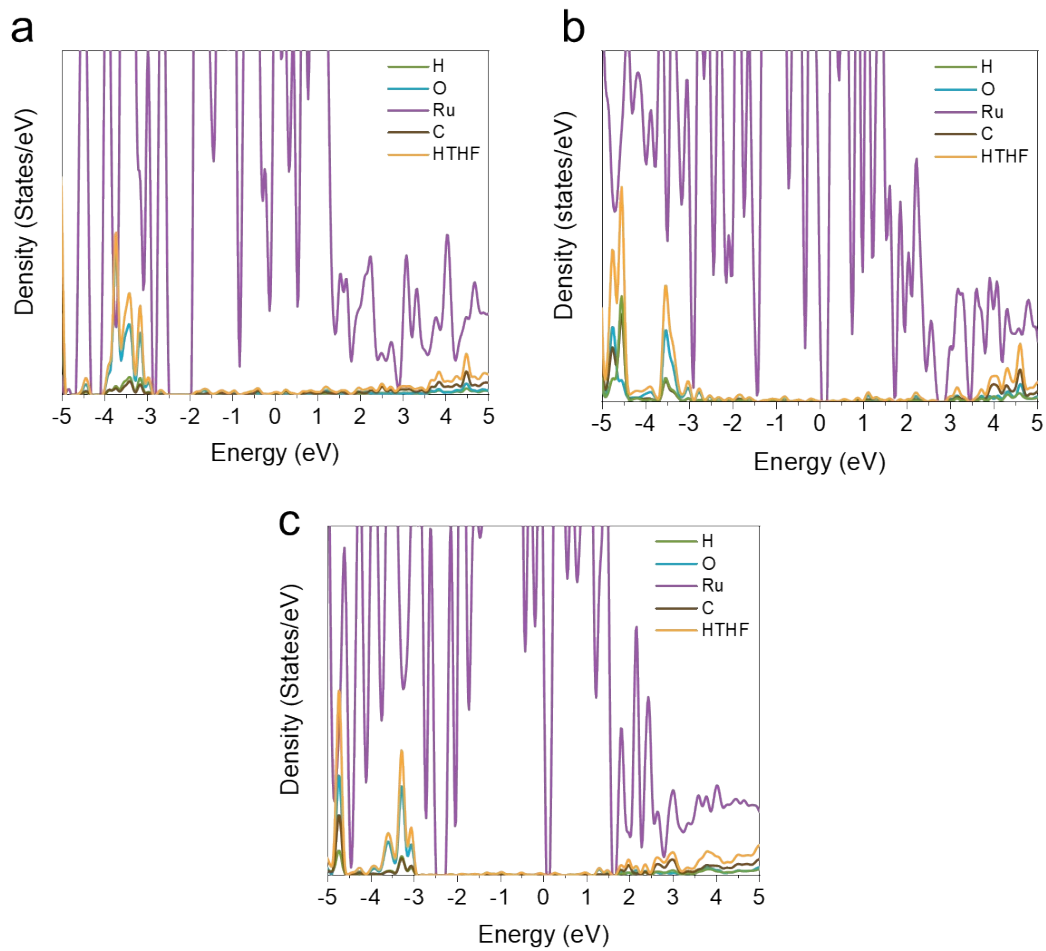


Figure S12. Density of states (DOS) of plots for (a) Ru/HT, (b) Ru/SiO<sub>2</sub>, (c) Ru/HAP model surface, respectively.

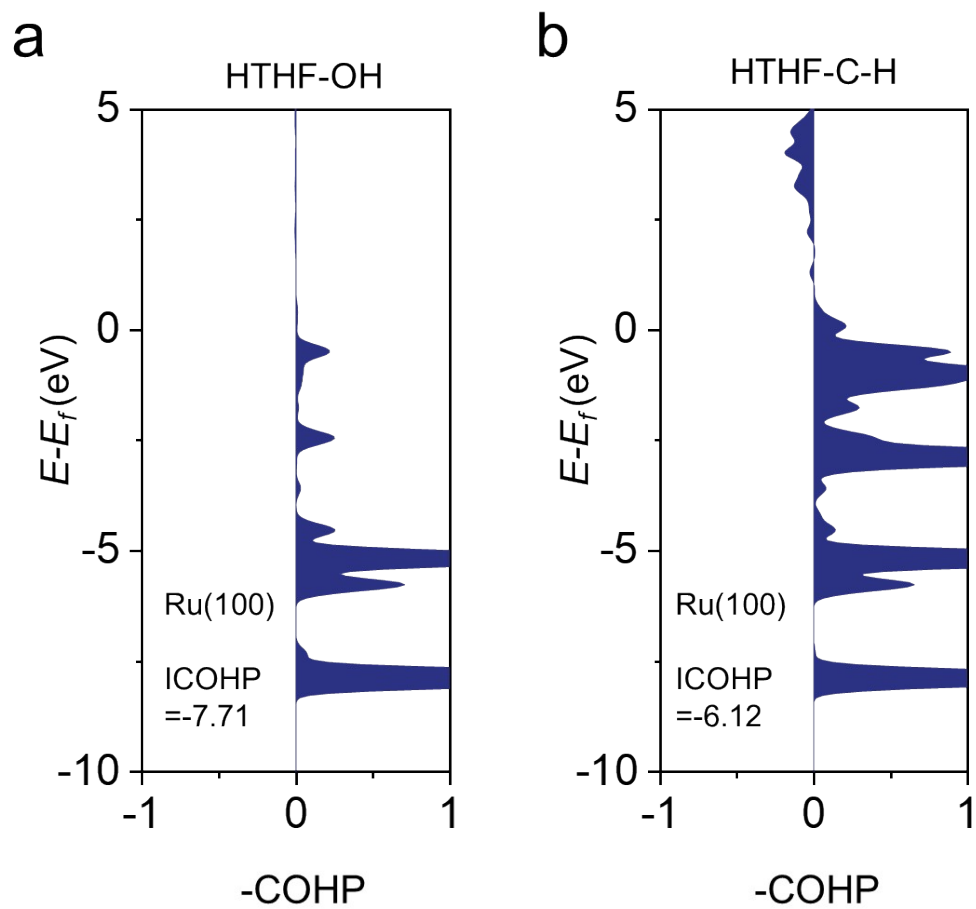


Figure S13. ICOHP values for the (a) O–H and (b) C–H bond in the adsorption configuration of 2-HTHF on the Ru(100) model surface, respectively.

**Table S1** Structural properties and crystallite size of the different catalysts

Samples	Ru loading (wt %) <sup>a</sup>	Dispersion (%) <sup>b</sup>	Surface area (m <sup>2</sup> g <sup>-1</sup> ) <sup>c</sup>	Pore diameter (nm) <sup>c</sup>	Pore volume (cm <sup>3</sup> g <sup>-1</sup> ) <sup>c</sup>
Ru/HT	3.93	19	3.93	9.90	0.000204
Ru/SiO <sub>2</sub>	4.02	20	4.90	4.20	0.000389
Ru/TiO <sub>2</sub>	4.17	16	61.5	34.3	0.002869
Ru/HAP	4.39	17	18.6	21.7	0.001354

<sup>a</sup>detected by inductively-coupled plasma optical emission spectroscopy (ICP-OES).

<sup>b</sup>Ru dispersion determined by CO pulse chemisorption.

<sup>c</sup>Surface area, pore diameter, and volume were determined by N<sub>2</sub> physisorption measurements.

**Table S2** Comparison of catalyst performance of Ru/TiO<sub>2</sub> with the representative ones reported in the literature in terms of activity in the aerobic oxidation reaction of aliphatic alcohols.

Catalysts	Reaction condition	BDO Con. (%)	2-HTHF Sel. (%)	TOF (h <sup>-1</sup> )	References
Ru/HT	0.5 MPa, 120 °C	52	96	451	This work
Ru/SiO <sub>2</sub>	0.5 MPa, 120 °C	66	93	552	This work
Ru/TiO <sub>2</sub>	0.5 MPa, 120 °C	99	97	1043	This work
Ru/HAP	0.5 MPa, 120 °C	99	70	846	This work
Au/TiO <sub>2</sub>	1.25 MPa, 120 °C	>99	1	64	Ref. <sup>1</sup>
Au/α-Fe <sub>3</sub> O <sub>4</sub>	1.25 MPa, 140 °C	100	14	207	Ref. <sup>2</sup>
Pd/TiO <sub>2</sub>	0.1 MPa, 90 °C	30	90	9	Ref. <sup>3</sup>
5%Pd/C	0.3 MPa, 50 °C	95	23	500	Ref. <sup>4</sup>
Pt/TiO <sub>2</sub>	0.1 MPa, 90 °C	30	15	405	Ref. <sup>3</sup>
Cu/Al <sub>2</sub> O <sub>3</sub>	0.1 MPa, 200 °C	100	2	18	Ref. <sup>5</sup>
Cu/MgO-CeO <sub>2</sub>	0.1 MPa, 240 °C	100	1	12	Ref. <sup>6</sup>
0.5%Cu-1.0%Pt/AC	0.1 MPa, 90 °C	80	31	437	Ref. <sup>7</sup>
Ru <sup>3+</sup> -hydroxyapatite	0.1 MPa, 80 °C	95	6	0.4	Ref. <sup>8</sup>
PNP-type Ru (II)	0.1 MPa, 110 °C	96	4	17	Ref. <sup>9</sup>
1.4%Ru/Al <sub>2</sub> O <sub>3</sub>	0.1 MPa, 150 °C	none	none	300	Ref. <sup>10</sup>
Ru <sub>0.35</sub> MnFe <sub>1.5</sub> Cu <sub>0.15</sub> O <sub>x</sub>	0.1 MPa, 22 °C	90	0	3	Ref. <sup>11</sup>

**Table S3** Catalytic performance of the catalysts with different Ru loadings

Ru loading (wt %)	BDO Con.% <sup>a</sup>	2-HTHF Sel.%	GBL Sel.%
2.0 wt%	65.3	95.1	4.9
4.0 wt%	76.9	94.6	5.4
6.0 wt%	99.0	96.7	3.3
8.0 wt%	94.3	98.3	1.7

<sup>a</sup> Reaction conditions: 100 mg BDO, 30 mg catalyst, 10 mL TBP, 120 °C, 0.5 MPa O<sub>2</sub>, 6h, 800 rpm.

1. Huang, J.; Dai, W.-L.; Li, H.; Fan, K., Au/TiO<sub>2</sub> as high efficient catalyst for the selective oxidative cyclization of 1,4-butanediol to  $\gamma$ -butyrolactone. *Journal of Catalysis* **2007**, *252* (1), 69-76.
2. Huang, J.; Dai, W.-L.; Fan, K., Remarkable support crystal phase effect in Au/FeO<sub>x</sub> catalyzed oxidation of 1,4-butanediol to  $\gamma$ -butyrolactone. *Journal of Catalysis* **2009**, *266* (2), 228-235.
3. Shen, Y.; Zhang, S.; Li, H.; Ren, Y.; Liu, H., Efficient Synthesis of Lactic Acid by Aerobic Oxidation of Glycerol on Au–Pt/TiO<sub>2</sub> Catalysts. *Chemistry – A European Journal* **2010**, *16* (25), 7368-7371.
4. Hu, T.; Wang, J.; Xie, Y.; Cao, F.; Jia, L.; Wu, X.; Sun, G., Silver incorporated into tunneled manganese oxide promotes hydrogen production from aqueous formaldehyde. *Appl. Surf. Sci.* **2022**, *589*, 152908.
5. Soumya Reddy, M.; Madhu Krushna, B.; Venkata Rao, M.; Srinivasu, P., Architecture of bimodal porous CuO/Al<sub>2</sub>O<sub>3</sub>-controlled continuous and low-temperature production of biomass-derived  $\gamma$ -butyrolactone. *Chemical Engineering Journal* **2024**, *498*, 155062.
6. Chong, S.; Zhao, S.; Li, J.; Huang, G.; Zhang, Y.; Liu, R.; Wang, K., Enhanced the dehydrocyclization of 1,4-butanediol to  $\gamma$ -butyrolactone via the regulation of interface oxygen vacancies in Cu/MgO-CeO<sub>2</sub> catalyst. *Chemical Engineering Journal* **2024**, *489*, 151366.
7. Zhang, C.; Wang, T.; Liu, X.; Ding, Y., Cu-promoted Pt/activated carbon catalyst for glycerol oxidation to lactic acid. *Journal of Molecular Catalysis A: Chemical* **2016**, *424*, 91-97.
8. Yamaguchi, K.; Mori, K.; Mizugaki, T.; Ebitani, K.; Kaneda, K., Creation of a Monomeric Ru Species on the Surface of Hydroxyapatite as an Efficient Heterogeneous Catalyst for Aerobic Alcohol Oxidation. *Journal of the American Chemical Society* **2000**, *122* (29), 7144-7145.
9. Zhang, J.; Balaraman, E.; Leitens, G.; Milstein, D., Electron-Rich PNP- and PNN-Type Ruthenium(II) Hydrido Borohydride Pincer Complexes. Synthesis, Structure, and Catalytic Dehydrogenation of Alcohols and Hydrogenation of Esters. *Organometallics* **2011**, *30* (21), 5716-5724.
10. Mallat, T.; Baiker, A., Oxidation of Alcohols with Molecular Oxygen on Solid Catalysts. *Chemical Reviews* **2004**, *104* (6), 3037-3058.
11. Ji, H.-B.; Ebitani, K.; Mizugaki, T.; Kaneda, K., Environmentally friendly alcohol oxidation using heterogeneous catalyst in the presence of air at room temperature. *Catalysis Communications* **2002**, *3* (11), 511-517.